Analysis of Coulomb breakup experiments of ^{8}B with a dynamical eikonal approximation

G. Goldstein,[1,*] P. Capel,[1,†] and D. Baye[1,‡]

[1] *Physique Quantique, C.P. 165/82 and Physique Nucléaire Théorique et Physique Mathématique, C.P. 229, Université Libre de Bruxelles, B 1050 Brussels, Belgium*

(Dated: February 1, 2008)

Various measurements of the Coulomb breakup of ^{8}B are analysed within the dynamical eikonal approximation using a single description of ^{8}B. We obtain a good agreement with experiment for different observables measured between 40 and 80 MeV per nucleon. A simple ^{7}Be-p potential model description of ^{8}B seems sufficient to describe all observables. In particular, the asymmetry in parallel-momentum distributions due to $E1$-$E2$ interferences is well reproduced without any scaling. The projectile-target nuclear interactions seem negligible if data are selected at forward angles. On the contrary, like in previous analyses we observe a significant influence of higher-order effects. The accuracy of astrophysical S factors for the ^{7}Be$(p,\gamma)^8$B reaction at stellar energies extracted from breakup measurements therefore seems difficult to evaluate.

PACS numbers: 24.10.-i, 25.60.Gc, 25.70.De, 25.40.Lw
Keywords: Coulomb dissociation, ^{8}B, astrophysical factor S_{17}

arXiv:0708.0357v1 [nucl-th] 2 Aug 2007

I. INTRODUCTION

The ^{7}Be$(p,\gamma)^8$B radiative capture reaction is one of the key reactions for understanding neutrino properties [1]. Indeed, the main part of high energy neutrinos emitted by the sun arise from this reaction. Its properties determine our knowledge of neutrino oscillations.

The capture of protons by ^{7}Be has been studied by many direct measurements (see Refs. [2, 3, 4] and references therein). However the difficulty of these measurements and the scatter of their results has raised interest in indirect methods where the time-reversed reaction is simulated by virtual photons in the Coulomb field of a heavy nucleus [5]. The radiative capture cross section can be extracted if one assumes that the breakup is due to an E1 virtual photon and occurs in a single step. Several experiments have studied the breakup of ^{8}B at different energies [6, 7, 8, 9, 10, 11].

Though appealing, the breakup method also faces a number of difficulties. First, while the reaction ^{7}Be$(p,\gamma)^8$B is dominated by an E1 transition, the E2 contribution to the breakup of ^{8}B is not negligible [12]. Second, higher-order effects, i.e. transitions from the initial bound state into the continuum through several steps are not negligible [12]. Finally, the nuclear interactions between ^{8}B and the target may interfere with the Coulomb interaction. Therefore elaborate reaction theories must be used to interpret the experimental data. Such

*Electronic address: gerald.goldstein@ulb.ac.be
†Electronic address: pierre.capel@centraliens.net
‡Electronic address: dbaye@ulb.ac.be

calculations have been performed with perturbation theories [12, 13], DWBA [14], semi-classical methods [12, 15, 16, 17], and the continuum-discretized coupled channels (CDCC) method [18, 19, 20].

A few years ago, we have developed a technique of resolution of the semi-classical time-dependent Schrödinger equation on a mesh in spherical coordinates [21, 22, 23]. This calculation on a mesh avoids partial wave expansions of the wave functions and a multipole expansion of the interaction. We have used this method to explore certain aspects of the extraction of the astrophysical S factor from breakup cross sections [23, 24].

Recently, we have developed a purely quantal method based on the same semi-classical code, the dynamical eikonal approximation (DEA) [25, 26]. This method allows taking into account purely quantal effects such as interferences, as well as calculating differential cross sections.

The purpose of this paper is to analyze ^{8}B breakup on a lead target within the DEA. Until now, theoretical works have focused on a single experiment, i.e. the RIKEN experiment at 52 MeV/nucleon [7] or the MSU experiments at 44 and 81 MeV/nucleon [8], and 83 MeV/nucleon [10]. Here we address both experiments within exactly the same model, without any fit of parameters. The theoretical model will then serve as a link between those experiments. We do not consider the GSI experiment [11] because it is performed at a much higher energy where relativistic effects become important. The present study is nonrelativistic, except for kinematical effects, before and after the reaction, which are treated relativistically. Neither will we analyse the Notre-Dame experiment [9]. It has been performed at sub-Coulomb energies, where the DEA is not reliable.

In Sec. II, we summarize the DEA, describe the cross section formulas in the center-of-mass and laboratory frames and present our treatment of relativistic corrections. The condition of the calculations, including the description of the projectile and numerical inputs, are given in Sec. III. In Sec. IV, the results are presented and commented, and the accuracy of the extraction of the astrophysical S factor is discussed. Sec. V is devoted to concluding remarks.

II. DYNAMICAL EIKONAL APPROXIMATION

A. Principle

We are interested in describing a reaction in which a two-body projectile P made up of a structureless core c, with mass m_c and charge $Z_c e$, and a structureless fragment f, with mass m_f and charge $Z_f e$, is broken up after its interaction with a target T, with mass m_T and charge $Z_T e$. Since the target state remains unchanged, this process is also called elastic breakup. We work in Jacobi coordinates where $\boldsymbol{R}$ is the coordinate of the center of mass of the projectile with respect to the target and $\boldsymbol{r}$ is the coordinate of the fragment with respect to the core. The corresponding momenta are $\boldsymbol{P}$ and $\boldsymbol{p}$, respectively. The projectile is described by an internal Hamiltonian

$$H_0 = \frac{p^2}{2\mu_{cf}} + V_{cf}(\boldsymbol{r}), \tag{1}$$

where μ_{cf} is the core-fragment reduced mass. Hamiltonian H_0 is composed of the kinetic energy operator for the relative motion between core and fragment and of the core-fragment

interaction potential. The potential V_{cf} contains an angular-momentum dependent central term (including a Coulomb interaction) and a spin-orbit term involving the fragment spin. The spin of the core is neglected. The eigenstates of H_0 with energy E are denoted as $\phi_{ljm}(E, \boldsymbol{r})$, where j is the angular momentum resulting from the coupling of the orbital momentum l with the fragment spin I and m is its projection. The projectile is initially in its ground state $\phi_{l_0 j_0 m_0}(E_0, \boldsymbol{r})$ and the asymptotic projectile-target relative velocity is given by v.

With these assumptions, the system is described by the three-body Schrödinger equation

$$\left[\frac{P^2}{2\mu} + H_0 + V_{cT}(\boldsymbol{r}, \boldsymbol{R}) + V_{fT}(\boldsymbol{r}, \boldsymbol{R})\right] \Psi(\boldsymbol{r}, \boldsymbol{R}) = E_T \Psi(\boldsymbol{r}, \boldsymbol{R}), \tag{2}$$

where μ is the projectile-target reduced mass and E_T is the total internal energy of the three-body system. Optical potentials V_{cT} and V_{fT} simulate the core-target and fragment-target interactions, respectively. In the DEA [25, 26], after posing $\Psi(\boldsymbol{R}, \boldsymbol{r}) = \exp(iKZ)\hat{\Psi}(\boldsymbol{R}, \boldsymbol{r})$, we apply the eikonal approximation, i.e. we neglect second derivatives of $\hat{\Psi}$ which are small at high velocities. We do however not perform the adiabatic approximation, i.e. H_0 is not replaced by E_0. The resulting equation looks like the semiclassical time-dependent Schrödinger equation with straight lines trajectories

$$i\hbar \frac{\partial}{\partial t} \hat{\Psi}(\boldsymbol{r}, \boldsymbol{b}, t) = [H_0(\boldsymbol{r}) + V_{cT}(\boldsymbol{r}, \boldsymbol{b}, t) + V_{fT}(\boldsymbol{r}, \boldsymbol{b}, t) - E_0] \hat{\Psi}(\boldsymbol{r}, \boldsymbol{b}, t). \tag{3}$$

In this equation, the variable t is linked to the part of the quantal coordinate $\boldsymbol{R}$ parallel to the incident direction $Z = vt$, while the vector $\boldsymbol{b} = (b, \phi)$ represents the transverse part of $\boldsymbol{R}$. Its norm b can be assimilated to the semiclassical impact parameter. In theory, this equation must be solved for all values of b and ϕ, but we will see that only one arbitrary value of ϕ is actually needed.

Let $\hat{\Psi}^{(m_0)}(\boldsymbol{r}, b, t)$ be a particular solution of equation (3) corresponding to the initial condition $\hat{\Psi}^{(m_0)}(\boldsymbol{r}, b, t) \underset{t \to -\infty}{\to} \phi_{l_0 j_0 m_0}(E_0, \boldsymbol{r})$ and to the particular orientation $\phi = 0$. In the basis $|lIjm\rangle$ coupling the orbital momentum l and the fragment spin I, the asymptotic form of this solution reads

$$\lim_{t \to +\infty} \hat{\Psi}^{(m_0)}(\boldsymbol{r}, b, t) = \frac{1}{r} \sum_{ljm} \psi_{ljm}^{(m_0)}(r, b, 0) \langle \Omega_r | lIjm \rangle. \tag{4}$$

¿From this solution, one can derive the solutions for $\phi \neq 0$ using

$$\psi_{ljm}^{(m_0)}(r, b, \phi) = e^{i(m_0 - m)\phi} \psi_{ljm}^{(m_0)}(r, b, 0). \tag{5}$$

The whole information needed to extract cross sections is contained in the breakup amplitude given by [26]

$$S_{kljm}^{(m_0)}(b) = e^{i(\sigma_l + \delta_{lj} - l\pi/2)} \int_0^\infty u_{klj}(r) \psi_{ljm}^{(m_0)}(r, b, 0) dr, \tag{6}$$

where σ_l and δ_{lj} are the Coulomb and nuclear phase shifts at positive energy $E = \hbar^2 k^2 / 2\mu_{cf}$. The functions $u_{klj}(r)$ are the radial parts of eigenstates of H_0 at energy E. They are normalized according to

$$u_{klj}(r) \underset{r \to \infty}{\longrightarrow} \cos \delta_{lj} F_l(kr) + \sin \delta_{lj} G_l(kr), \tag{7}$$

where F_l and G_l are the Coulomb functions [27].

B. Cross sections in the center of mass frame

In the center of mass frame of the projectile and the target, the breakup transition matrix element for final projectile-target wave vector $\boldsymbol{K'} = (K', \Omega) = (K', \theta, \varphi)$ within the DEA is given by [26, 28]

$$T_{fi}(\boldsymbol{k}, \Omega) = i8\pi^2 \frac{\hbar v}{k} \sum_{ljm} (lIm - \nu\nu|jm) Y_l^{m-\nu}(\theta_k, \varphi_k)$$
$$i^{-|m-m_0|} e^{i(m_0-m)\varphi} \int_0^\infty bdbJ_{|m-m_0|}(qb) S_{kljm}^{(m_0)}(b), \tag{8}$$

where ν is the projection of the fragment spin of the final state, (θ_k, φ_k) is the emission direction of the fragments of the projectile, and $q \approx 2K \sin(\theta/2)$ is the transfered momentum. The phase in equation (5) ensures the rotational symmetry around the Z-axis since the modulus of T_{fi} depends on $\varphi - \varphi_k$.

After integration over θ_k, and φ_k, these transition matrix elements lead to the differential cross section given by [26]

$$\frac{d\sigma}{dEd\Omega} = KK' \frac{2\mu_{cf}}{\pi\hbar^2 k} \frac{1}{2j_0+1} \sum_{m_0} \sum_{ljm} \left| \int_0^\infty bdbJ_{|m-m_0|}(qb) S_{kljm}^{(m_0)}(b) \right|^2, \tag{9}$$

where $K = \mu v/\hbar$. The sums over the $2j_0+1$ values of m_0 appearing in formulas (9) and (11) can be reduced to only positive or negative values of m_0 by using the following symmetry property

$$S_{kljm}^{(-m_0)}(b) = (-)^{l_0+j_0+m_0+l+j-m} S_{klj-m}^{(m_0)}(b). \tag{10}$$

C. Cross sections in the laboratory frame

Most experimental results are presented in the laboratory frame, so that a frame transformation from the center of mass frame must be performed. Let E_c, Ω_c, and Ω_f be the core energy, the core and fragment directions of emission, respectively. The cross section then reads

$$\frac{d\sigma}{dE_c d\Omega_c d\Omega_f} = \frac{2\pi}{\hbar v} \frac{1}{2j_0+1} \sum_{m_0\nu} |T_{fi}(\boldsymbol{k}, \Omega)|^2 \rho(E_c, \Omega_c, \Omega_f), \tag{11}$$

where $\rho(E_c, \Omega_c, \Omega_f)$ is the three-body phase space factor [29] given by Eq. (B7) (see also Ref. [18]). The transition matrix element T_{fi} is evaluated at values of $\boldsymbol{k}$ and Ω linked to the values of the core momentum $\boldsymbol{p}_c$ and the fragment momentum $\boldsymbol{p}_f$ in the laboratory frame, by

$$\hbar\boldsymbol{k} = \frac{m_c}{m_P}\boldsymbol{p}_f - \frac{m_f}{m_P}\boldsymbol{p}_c \tag{12}$$

$$\hbar\boldsymbol{K'} = \boldsymbol{p}_c + \boldsymbol{p}_f - \frac{m_P}{m_T + m_P}\boldsymbol{p}_{tot}, \tag{13}$$

where $\boldsymbol{p}_{tot} = m_P\boldsymbol{v}$ is the total momentum. Detailed expressions of the frame transformation are given in Appendix B. Notice that the transition matrix element T_{fi} must be calculated

for each $(\boldsymbol{k}, \Omega)$. In particular, for each couple (k, q), the breakup amplitude $S^{(m_0)}_{kljm}(b)$ and its integrals over b in Eq. (8) are recalculated.

We are also interested by the computation of the core parallel momentum distribution, so that the cross section (11) must be integrated three times using the following expression

$$\frac{d\sigma}{dp_{c\|}} = \frac{2\pi}{m_c} \int_{|p_{c\|}|}^{p_c^{\max}} dp_c \int_0^{\pi} d\theta_f \sin\theta_f \int_0^{2\pi} d\Delta\varphi \; \frac{d\sigma}{dE_c d\Omega_c d\Omega_f}, \tag{14}$$

where $p_c^{\max} = |p_{c\|}|/\cos\theta_c^{\max}$ and $\Delta\varphi = \varphi_c - \varphi_f$. Notice that the two integrations over φ_c and φ_f reduce to a single integration over $\Delta\varphi$ since $d\sigma/dE_c d\Omega_c d\Omega_f$ is a periodic function of $\Delta\varphi$ [see equations (8) and (B1) to (B7)]. As for the cross sections in the c.m. frame, the sum over m_0 can also be reduced using property (10). This is the case only when the cross sections is integrated over $\Delta\varphi$ like in expression (14).

D. Kinematical relativistic corrections

As mentioned in the Introduction, the present model is nonrelativistic like its basic equation (2). However, kinematical relativistic corrections are used before and after the reaction.

The velocity of the projectile v used for solving the time-dependent Schrödinger equation (3) is calculated using the relativistic formula

$$\frac{v}{c} = \sqrt{1 - \frac{1}{(1 + \frac{T_i}{m_P c^2})^2}}, \tag{15}$$

where T_i is the initial kinetic energy of the projectile and m_P its mass. This velocity is also used for the frame transformation. This is common practice.

In order to be consistent with our velocity choice, we use at the end of the calculation the inverse relation for the parallel momentum, i.e. we associate to each observed momentum $\boldsymbol{p}_c$ a non-relativistic value $\boldsymbol{p}_c^{NR}$. The parallel component of this nonrelativistic momentum $p_{c\|}^{NR}$ at which the cross section must be computed to simulate the actual one $p_{c\|}$ is

$$p_{c\|}^{NR} = \left(\frac{1}{(m_P c)^2} + \frac{1}{p_{c\|}^2} \right)^{-1/2}, \tag{16}$$

while its transverse component remains unchanged. Hence the non relativistic emission angles θ_c^{NR} giving the direction of the final momentum are obtained according to

$$\tan\theta_c^{NR} = \frac{p_{c\|}}{p_{c\|}^{NR}} \tan\theta_c. \tag{17}$$

This reduction will in particular affect the cutoff angles.

III. CONDITION OF CALCULATIONS

A. Description of ^{8}B

The spectrum of ^{8}B contains only one bound state with $J^\pi = 2^+$. It is bound by a mere 137 keV in regards to the one-proton separation. Therefore ^{8}B is usually seen as a

valence proton loosely bound to a ^{7}Be core. In the dominant configuration this proton is in a $0p3/2$ orbit coupled to the $\frac{3}{2}^-$ ground state of ^{7}Be [30]. For computational reasons, we restrict ourselves here to a simple model of ^{8}B, in which the spin and internal structure of the core are neglected. This description corresponds to the Hamiltonian H_0 given in Eq. (1). The ^{7}Be-p potential V_{cf} contains both Coulomb and nuclear terms. The former is a point-sphere Coulomb potential of radius $R_C = 2.391$ fm. The latter is a central Woods-Saxon potential plus a spin-orbit coupling term. Their radius and diffuseness are $R_0 = 2.391$ fm and $a = 0.52$ fm, respectively. The strength of the spin-orbit coupling term is $V_{LS} = 19.59$ MeV fm^2. The depth of the central nuclear potential V_0 is adjusted in order to reproduce the $0p3/2$ bound state at -137 keV. With $\hbar^2/2\mu_{cf} = 23.698$ MeV fm^2, we obtain $V_0 = 44.65$ MeV. This ^{8}B description corresponds to a simplified version of the model of Esbensen and Bertsch [12]. It has been used in previous dynamical calculations of ^{8}B breakup [12, 18, 19, 31].

The simplicity of this structure model has several drawbacks. First, since the spin of the core is neglected, it is not possible to adjust the ^{7}Be-p interaction to reproduce the scattering length in both $S = 1$ and $S = 2$ total-spin channels. Choosing the same V_{cf} potential in all partial waves gives $a_0 = 5.9$ fm, in between the (large) positive value of the $S = 1$ channel (25 ± 9 fm) and the negative value of the $S = 2$ channel (-7 ± 3 fm) [32]. Second, the absence of core spin means that all 0^+, 1^+, and 3^+ states corresponding to the coupling of this spin with the 3/2 angular momentum of the proton are degenerate with the 2^+ ground state. In particular, the 1^+ resonance located 632 keV above the proton separation threshold is not reproduced by this model. Finally, the structure of the core being neglected, no process leading to its excitation can be simulated.

B. Projectile-target interactions

The nuclear interactions between the projectile constituents and the target are simulated with optical potentials chosen in the literature. Unfortunately, no scattering data are available for the elastic scattering of ^{7}Be on Pb at energies of interest. Following Mortimer, Thompson, and Tostevin [19], we consider the potential developed by Cook [33]. It is a global parametrization determined from elastic scattering data of ^{7}Li on various targets at different energies. To describe the p-Pb interaction, we use the parametrization of Becchetti and Greenlees [34], neglecting the spin-orbit coupling term.

C. Numerical inputs

The time-dependent Schrödinger equation obtained from the DEA (3) is solved using the numerical technique detailed in Ref. [21]. In this technique, the projectile internal wave function is expanded upon a three-dimensional spherical mesh. The angular grid contains up to $N_\theta = 10$ points along the colatitude θ, and $N_\varphi = 19$ points along the azimuthal angle φ. This corresponds to an angular basis that includes all possible spherical harmonics up to $l = 9$. The radial variable r is discretized on a quasiuniform mesh that contains $N_r = 800$ points and extends up to $r_{N_r} = 800$ fm. The evolution calculation is performed with a second-order approximation of the evolution operator. It is started at $t_{\rm in} = -20$ $\hbar$/MeV with the projectile in its initial bound state, and is stopped at $t_{\rm out} = 20$ $\hbar$/MeV ($t = 0$ corresponds to the time of closest approach). The time step is set to $\Delta t = 0.04\hbar$/MeV.

The evolution calculations are performed for different values of the transverse component b of the projectile-target coordinate (see Sec. II A). These values range from 0 up to 200 fm with a step Δb varying from 0.5 fm to 5.0 fm, depending on b. The integrals over this impact parameter appearing in Eqs. (8), and (9) are performed numerically. To take into account the rapid variation of the Bessel function, the values of the breakup amplitude $S^{(m_0)}_{kljm}$ are interpolated on a uniform grid in b with a step of 0.05 fm. The convergence of these integrals is ensured by extrapolating the $S^{(m_0)}_{kljm}$ up to $b = 500$ fm as explained in Sec. III A of Ref. [26].

IV. ANALYSIS OF EXPERIMENTS

A. Longitudinal momentum distribution

The longitudinal momentum distribution (14) of ^{7}Be obtained from the dissociation of ^{8}B on lead at incident energies of 44 and 81 MeV/nucleon has been measured at MSU [8, 31]. These measurements have been performed with the aim of evaluating the contribution of the $E2$ strength in Coulomb breakup. This observable is indeed the best suited to measure the influence of the electric quadrupole transition since, as shown by Esbensen and Bertsch [12], $E1$-$E2$ interferences produce a significant asymmetry in that distribution.

The results of our calculations are displayed alongside the experimental data in Fig. 1 for the breakup of ^{8}B on lead at 44 MeV/nucleon. Each set of curves corresponds to a given cut in the scattering angle θ_c of ^{7}Be: the upper one is obtained for $\theta_c < 6°$; the lower ones correspond to the experimental angle cuts $\theta_c < 3.5°$, $2.4°$, and $1.5°$. To allow the comparison with experiment, our calculations have been convoluted with the experimental resolution of 5 MeV/c [8]. They have also been shifted by -5 MeV/c so as to be centered on the data. It can be seen as a fine adjustment to the data not taken into account by the relativistic corrections (see Sec. II D). This shift is very small compared to the central value of the longitudinal momentum (2025 MeV/c). Moreover it is equal to the experimental resolution. The relativistic corrections (16)-(17) used to calculate the parallel momentum in the laboratory frame thus seem efficient. Finally, note that no other parameter fitting has been performed. In particular, the magnitude of the curves is exactly that obtained from our calculations.

The full lines (labeled C.+N.) in Fig. 1 correspond to calculations performed with realistic projectile-target (P-T) interactions, i.e. using optical potentials that simulate both Coulomb and nuclear interactions (see Sec. III B). These results are in very good agreement with the data at the three forward angle cuts. They match both the magnitude and width of the experimental distributions. Moreover, they reproduce fairly well the asymmetry observed by Davids *et al.* [8]. This is particularly true at the smallest angle cut, where our calculations are nearly superimposed on the data. Note that with a cutoff on θ_c at 6°, the distribution exhibits very little asymmetry.

These results confirm the validity of the DEA to describe the dissociation of loosely-bound projectiles at intermediate energies, as already observed for the dissociation of ^{11}Be [25, 26]. Moreover they imply that the simple model of ^{8}B is sufficient to describe this breakup observable.

To better understand the reaction mechanism, as well as analyse the role of each interaction in the dissociation, the calculations are performed with different choices of P-T potentials. First, we consider a purely Coulomb interaction. These results are shown as

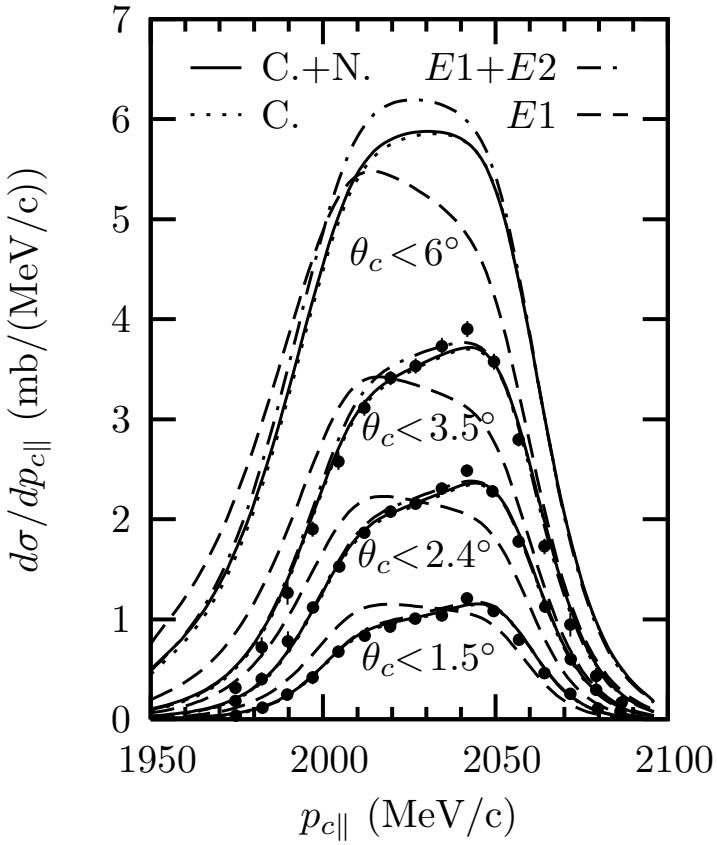

FIG. 1: Longitudinal momentum distributions of ^{7}Be obtained by dissociation of ^{8}B on Pb at 44 MeV/nucleon. The upper set of curves corresponds to ^{7}Be scattering-angle cut $\theta_c < 6°$. The lower three, along with the experimental data [8], correspond to $\theta_c < 3.5°$, 2.4°, and 1.5°. DEA calculations are performed using Coulomb plus nuclear (full lines), purely Coulomb (dotted lines), $E1 + E2$ (dash-dotted lines), and $E1$ (dashed lines) P-T interactions. All distributions are convoluted with the experimental resolution of 5 MeV/c. For comparison with the data they are also shifted by -5 MeV/c.

dotted lines in Fig. 1 (labeled C.). They are barely distinguishable from the previous ones (even for $\theta_c < 6°$), which indicates that P-T nuclear interactions are negligible when data are restricted to forward angles. The calculations can therefore be performed with a purely Coulomb interaction as done by Davids and Typel [15]. This avoids the uncertainty due to the choice of optical potentials.

The insensitivity to optical potentials also indicates that there is no absorption from the elastic-breakup channel at forward angles. This justifies the use of reaction models in which only elastic breakup is considered to analyse the inclusive measurements of Davids *et al.* [8], where the valence proton is not detected in coincidence with the ^{7}Be core.

To evaluate the influence of the different multipoles of the Coulomb interaction, we also perform DEA calculations considering only the dipole term ($E1$), and the sum of the dipole and quadrupole terms ($E1 + E2$). The results obtained with the purely $E1$ interaction (dashed lines) confirm the previous analyses [8, 12, 15, 19, 31]: $E1$ strength alone is not able to reproduce the data. In particular, this calculation exhibits a reverse asymmetry

compared with the data, even at very forward angles. The quadrupole term of the Coulomb interaction is therefore mandatory to correctly interpret the data. We see indeed that the results obtained with both dipole and quadrupole terms (dash-dotted lines) are in better agreement with the data. Note that we still observe some slight difference with the full calculation. This difference becomes negligible at very small θ_c. It is probably due to higher multipoles. In a semiclassical viewpoint, their contributions indeed decrease at small scattering angle (i.e. large impact parameter) [35].

We now compare the DEA to the first-order perturbation theory (FO) [35]. In the latter approximation, the time-dependent Schrödinger equation (3) is solved perturbatively assuming straight-line trajectories, and purely Coulomb P-T interaction. This potential is expanded in a series of multipoles $E\lambda$, whose contributions to the breakup amplitude $S_{kljm}^{(m_0)E\lambda}(b)$ is given within the far-field approximation by Eq. (A1). The corresponding parallel-momentum distributions are computed assuming the classical relation between the impact parameter b and the scattering angle θ of the ^{8}B center of mass [35]. The comparison is made in Fig. 2. As in Fig. 1, the full lines depict the DEA results obtained considering both Coulomb and nuclear interactions between the projectile and the target (C.+N.). The dashed lines correspond to the first-order calculations performed with only the dipole term of the Coulomb interaction (FO $E1$). The first-order calculations obtained using dipole and quadrupole strengths are plotted as dot-dashed lines (FO).

At the first-order approximation, the $E1$ distribution shows no asymmetry. This is very different from the dynamical calculation, which shows a reverse asymmetry compared with the data (see dashed curves in Fig. 1). The difference is due to higher-order effects, which are neglected at the first-order of the perturbation theory. Such a substantial effect of higher-orders is in complete agreement with previous analyses that indicate a strong coupling between partial waves inside the continuum [17, 24]. An analysis of this experiment ignoring these effects seems therefore unrealistic.

Once the quadrupole term is included, even first-order theory leads to an asymmetric distribution. However, as already noted by previous studies, this is too strong an asymmetry [12, 15, 19, 31]: higher-order effects tend to reduce the asymmetry. This tendency is of course to be related to the reversal of the asymmetry observed for the purely $E1$ case. It confirms the necessity of taking into account dynamical effects to analyse the data.

We perform a similar analysis of the 81 MeV/nucleon data of Davids *et al.* [8]. Fig. 3 depicts the results of our calculations alongside the measurements. As for the 44 MeV/nucleon case, our longitudinal momentum distributions have been convoluted with the experimental resolution of 5 MeV/c [8]. We also need to shift our calculations to center them on the data. This shift (-9 MeV/c) is larger than for the 44 MeV/nucleon distributions, probably denoting larger relativistic corrections, which are less well simulated by our purely kinematical corrections (see Sec. II D). However it remains minor when compared with the average momentum and the experimental resolution.

The results of the full calculations (i.e. containing both Coulomb and nuclear P-T interactions) are plotted as full lines in Fig. 3. The agreement with experiment is less good than at 44 MeV/nucleon. The magnitude of the calculations is 10 to 25 % too high, depending on the angle cut, and its width is also larger than the experimental one. This could merely denote larger relativistic effects at this larger incident energy. It could also result form uncertainty in the data. The very good agreement with the 44 MeV/nucleon data might indeed be fortuitous, while the discrepancy observed at 81 MeV/nucleon might be more representative of the experimental uncertainty (e.g. on the angle cut). Nevertheless,

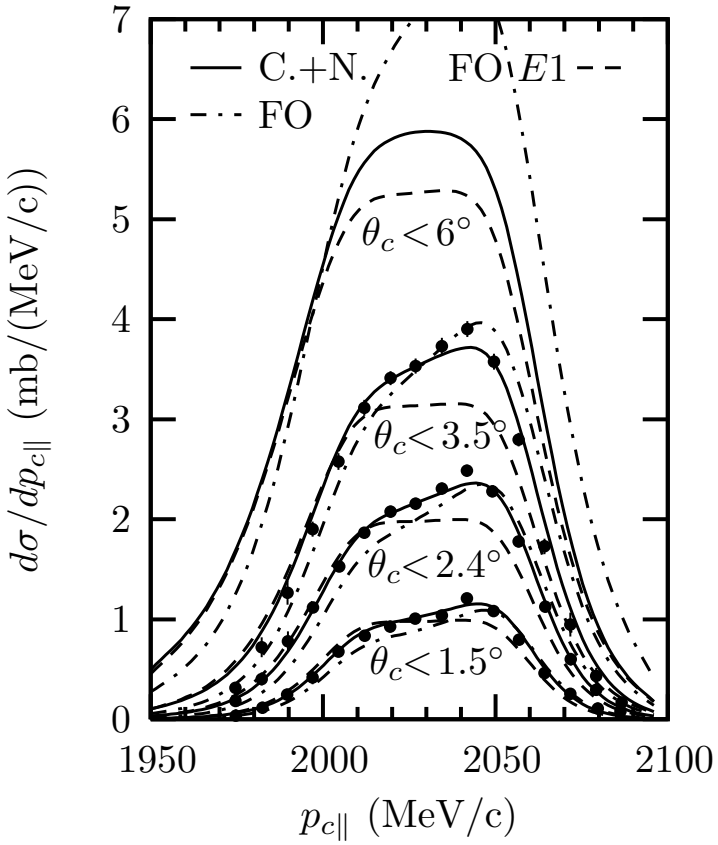

FIG. 2: Longitudinal momentum distributions of ^{7}Be obtained by dissociation of ^{8}B on Pb at 44 MeV/nucleon. Comparison of DEA and first-order (FO) calculations performed for angular cuts at 6°, 3.5°, 2.4°, and 1.5°. Experimental data are from Ref. [8]. DEA calculations are performed using Coulomb plus nuclear (full lines). First-order calculations are performed with $E1 + E2$ (dash-dotted lines) and $E1$ (dashed line) strengths. All distributions are convoluted with the experimental resolution of 5 MeV/c, and shifted by -5 MeV/c.

our distributions correctly reproduce the slope at the center of the distribution, which is usually the main concern of previous studies [8, 15, 19, 31].

As in the previous case, there is no significant influence of the nuclear interactions between the projectile components and the target. The calculations performed with purely Coulomb P-T interactions (dotted lines) are indeed very similar to those including nuclear optical potentials. In particular, all distributions have about the same width. Therefore the nuclear interaction cannot explain the too narrow widths obtained in Ref. [15], in contradiction with the authors' explanation.

The results obtained using only the $E1$ strength are depicted as dashed lines. Similarly to the previous case, we observe a reverse asymmetry when compared to the experiment. This is again a signature of the role in the dissociation process of both higher multipoles of the Coulomb interaction, and dynamical effects. This is confirmed by calculations performed at the first-order using both dipole and quadrupole strengths (dash-dotted lines). We indeed obtain a larger asymmetry than the fully dynamical calculation.

The calculations performed at 44 and 81 MeV/nucleon show both an asymmetry in

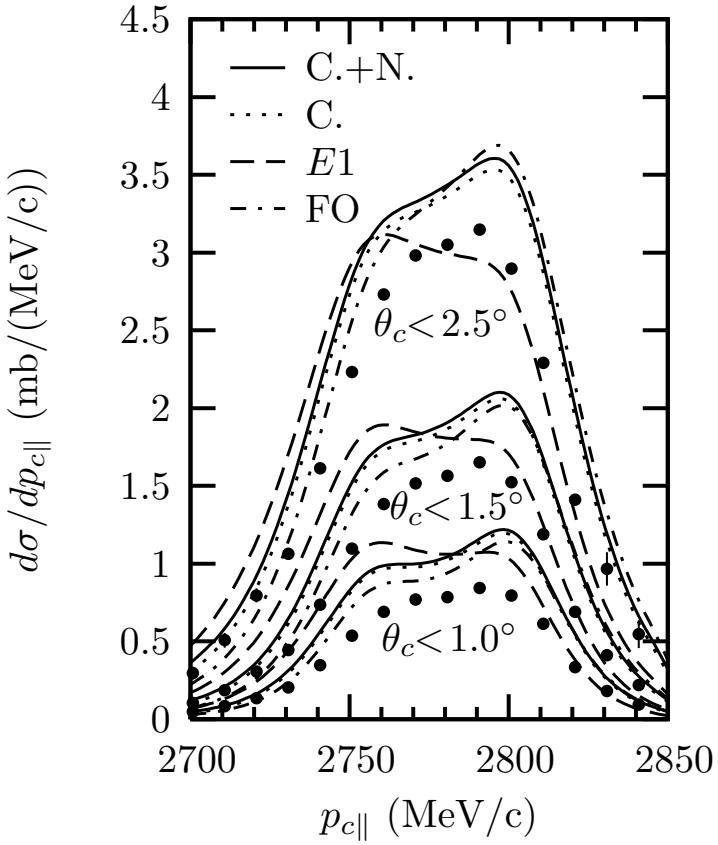

FIG. 3: Longitudinal momentum distributions of ^{7}Be obtained by dissociation of ^{8}B on Pb at 81 MeV/nucleon. The sets of results correspond to ^{7}Be scattering-angle cuts at 2.5°, 1.5°, and 1.0°. Experimental data are from Ref. [8]. DEA calculations are performed using Coulomb plus nuclear (full lines), purely Coulomb (dotted lines), and $E1$ (dashed lines) P-T interactions. First-order calculations are performed with $E1 + E2$ (dash-dotted lines) strengths. All distributions are convoluted with the experimental resolution of 5 MeV/c, and shifted by -9 MeV/c.

the ^{7}Be longitudinal-momentum distribution. In agreement with previous studies [12, 15, 19, 31], this asymmetry is found to be mainly due to interferences between dipole and quadrupole terms of the P-T Coulomb interaction. As already observed [12, 15, 19, 31] this asymmetry is reduced by higher-order effects. Using the simple description of ^{8}B of Esbensen and Bertsch [12] within the DEA [25, 26], we obtain a very good agreement with the experimental data of Davids *et al.* [8]. In particular, the asymmetry of the distribution is well reproduced at both energies. Contrarily to what has been suggested in previous calculations [8, 15, 19, 31], no scaling of the $E2$ strength is needed to explain the data. This suggests that the electromagnetic strengths given by the ^{8}B model of Esbensen and Bertsch is sufficient to describe the parallel-momentum distribution of the core obtained through Coulomb dissociation. To investigate further on the validity of this model, we now turn to other breakup observables.

B. Energy distribution

Consecutively to the aforementioned experiments, the breakup of ^{8}B on lead has been remeasured at MSU for an 83 MeV/nucleon incident beam [10]. Contrarily to the previous measurements, this one is exclusive in the sense that both the ^{7}Be core and the valence proton are detected in coincidence. This enabled Davids *et al.* to obtain the breakup cross section as a function of the ^{7}Be-p relative energy. The aim of this experiment was to extract the $B(E1)$ from this cross section using the first-order perturbation theory. This $E1$ strength was subsequently used to infer the astrophysical factor of the $^7\mathrm{Be}(p,\gamma)\,^8\mathrm{B}$ radiative capture at solar energy $S_{17}(0)$. Knowing the $E2$ strength not to be negligible, the authors used the $E2$ strength extracted from their previous measurements of the ^{7}Be longitudinal-momentum distribution [8]. In the present study, we consider these data as another breakup observable to which to compare our calculations.

Energy distributions obtained from the DEA are displayed in Fig. 4. Since the difference in incident energy is small, they are obtained from the 81 MeV/nucleon calculations. Like the experiment, they are limited to a scattering angle of the ^{8}B center of mass θ smaller than 1.77° [10]. For comparison with the data, the theoretical distributions ($d\sigma^{\mathrm{th}}/dE$) have been convoluted with the experimental energy resolution [36]

$$\frac{d\sigma^{\mathrm{conv}}}{dE}(E) = \int_0^\infty \frac{1}{\sqrt{2\pi}a(E')} \exp\left[-\frac{(E-E')^2}{2a(E')^2}\right] \frac{d\sigma^{\mathrm{th}}}{dE}(E')dE', \tag{18}$$

where the energy-dependent width a reads

$$a(E) = \begin{cases} 0.2072\sqrt{E} - 0.0145 & \text{if } E > 64 \text{ keV}, \\ 0.038 & \text{otherwise.} \end{cases} \tag{19}$$

In Eqs. (18), and (19), the energies E and E', and the width a, are expressed in MeV.

The full lines correspond to a calculation performed using realistic P-T interactions containing both Coulomb and nuclear potentials (see Sec. III B). The upper curve is the total cross section, while the lower curves correspond to partial wave contributions. The agreement with the experimental data is fair if one considers the very simple model of ^{8}B used here. The maximum of our theoretical distribution seems to be located slightly too low in energy in comparison with the data. The magnitude of our distribution, however, is similar to the experimental one. This suggests some contradiction between these data and those obtained at 81 MeV/nucleon, compared to which our calculations are too large by 10–25% (see Fig. 3).

As in Sec. IV A, we analyse the sensitivity of our calculation to the projectile-target interactions. The cross section obtained using purely Coulomb P-T interactions is shown as a dotted line. As for the longitudinal-momentum distributions, the difference with the calculation including both Coulomb and nuclear interactions is negligible. This confirms that for ^{8}B dissociation on a heavy target at intermediate energies, nuclear interactions can be neglected when observables are limited to forward angles.

The result obtained with only the dipole term of the Coulomb interaction (long-dashed line) confirms the less noticeable influence of higher multipoles in this observable. The shape is indeed similar whether the full interaction or only the $E1$ strength is considered.

In Fig. 4, we also compare our dynamical calculations with the first-order perturbation theory (dash-dotted lines). In the latter, the P-T interaction is purely Coulomb and is

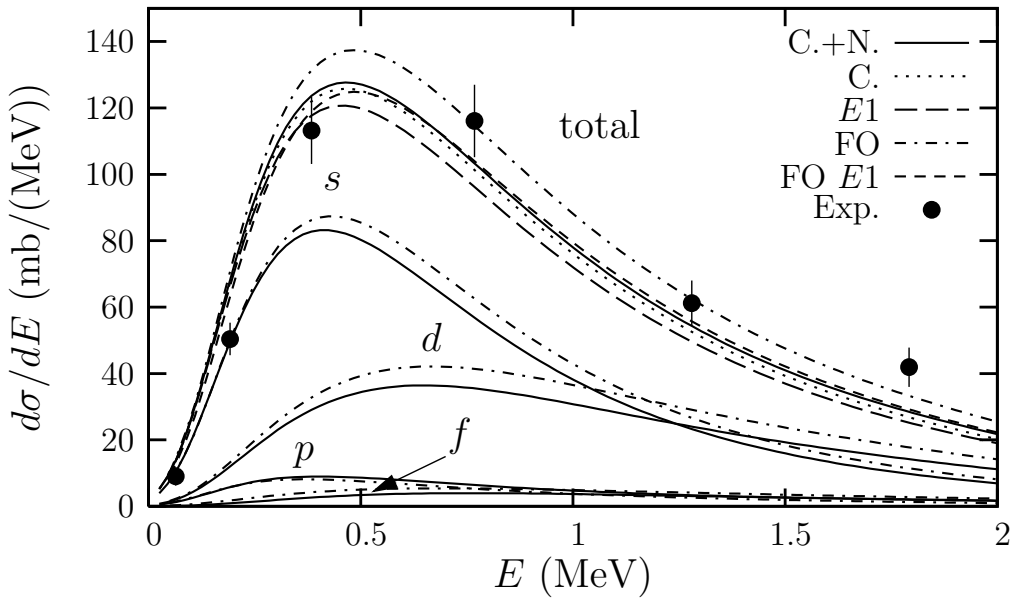

FIG. 4: Breakup of ^{8}B on Pb at 83 MeV/nucleon: relative energy distribution limited at forward ^{8}B scattering angles ($\theta \leq 1.77°$). Dynamical calculations are performed using Coulomb plus nuclear (full lines), purely Coulomb (dotted line), and $E1$ (long-dashed line) P-T interactions. First-order calculations are performed with $E1 + E2$ (dash-dotted lines) and $E1$ (short-dashed line) strengths. Some partial-wave contributions are also shown. Experimental data are from Ref. [10]. All distributions are convoluted with the experimental resolution [see Eq. (18)].

limited to its dipole and quadrupole terms. The scattering-angle cut is simulated by an impact-parameter cutoff at $b_{\min} = 30$ fm, as suggested in Ref. [10]. We observe a reduction between the first-order and dynamical calculations (9% at 0.5 MeV). A better agreement between the first-order and DEA total cross sections can be found using an impact-parameter cutoff at $b_{\min} = 34$ fm, which corresponds to the angular cut at 1.77° through the classical relation between b and θ [35]. In both cases significant higher-order effects are at play. We indeed observe that the variation between first-order and DEA is not the same in all partial waves (see lower curves in Fig. 4). While both dominant s and d contributions are reduced in the DEA calculation, the p contribution is slightly increased. In agreement with our previous analysis [24], we interpret this as couplings between different partial waves in the continuum. The variations observed here suggest that $E1$-$E1$ second-order transitions depopulate the s and d waves in the continuum towards the p and f waves, where they interfere with first-order $E2$ transitions. As already seen in Ref. [24], this effect varies with the relative energy E. It seems thus hazardous to model these higher-order effects as a mere reduction of the $E2$ strength within the first-order perturbation theory, as suggested in previous works [10, 15, 31]. These results confirm earlier studies [17, 24], which show that higher-order effects and $E2$ transitions interfere in ^{8}B Coulomb breakup, even at intermediate incident energies, and forward scattering angles.

Albeit fair, the agreement we obtain here between theory and experiment is less good than for the parallel-momentum distribution. One explanation for this difference might be the larger sensitivity of the energy distribution to the projectile continuum. Being integrated over the energies, the parallel-momentum distribution (14) might indeed be less sensitive to

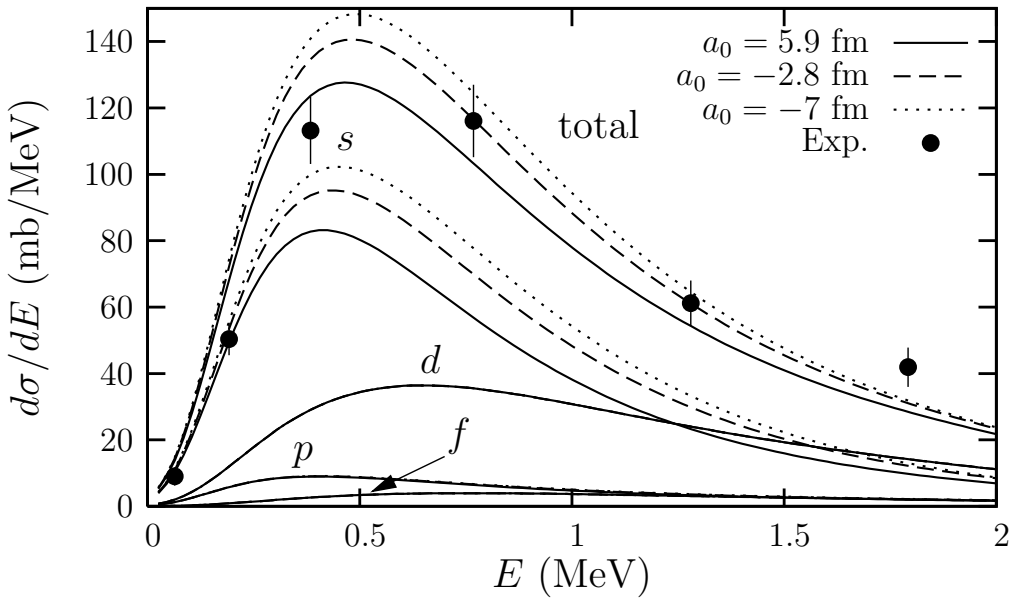

FIG. 5: Breakup of ^{8}B on Pb at 83 MeV/nucleon: influence of scattering length on breakup. Dynamical calculations with $a_0 = 5.9$ fm (initial potential; full lines), $a_0 = -2.8$ fm (dashed lines), and $a_0 = -7$ fm (dotted lines). Experimental data are from Ref. [10]. All distributions have been convoluted with the experimental resolution [see Eq. (18)].

that part of the projectile model. To investigate that possibility, we perform two additional calculations with ^{7}Be-p potentials adjusted in the s wave to reproduce various scattering lengths a_0. The potential is kept unchanged in all other partial waves. The corresponding energy distributions, as the major partial wave contributions are displayed in Fig. 5.

We first consider $a_0 = -2.8$ fm (dashed lines), which corresponds to the weighted average value between the scattering lengths for the total-spin channels $S = 1$ and $S = 2$ suggested in Ref. [37]. Second we fit the potential to $a_0 = -7$ fm (dotted lines), which is the value measured for the $S = 2$ channel [32]. Both calculations are performed considering Coulomb plus nuclear P-T interactions. The only variation we observe from the initial calculation ($a_0 = 5.9$ fm; full lines), is a significant increase of the magnitude of the s contribution. The shape of that contribution is similar for all potential choices. No significant change is observed in the other contributions. This result confirms the influence of the description of the projectile continuum upon breakup calculations [38, 39]. However, even adjusting scattering lengths on realistic values does not explain the difference observed between our calculations and experimental data. We suspect this observable to be more sensitive to the projectile description than momentum distributions. A more realistic model of ^{8}B, which takes into account the spin of the core, and reproduces the measured scattering lengths, might explain the slight shift observed in Fig. 4. However, such a model is still too time consuming for the DEA.

C. Angular distribution

In order to complete this analysis, we use the DEA to compute angular distributions and compare them to the data obtained by Kikuchi *et al.* at RIKEN [7]. In this experiment, the cross section for the breakup ^{8}B on lead at 52 MeV/nucleon has been measured as a function of the scattering angle θ of the ^{8}B center of mass. The main reason for this experiment was to evaluate the contribution of $E2$ transitions in the Coulomb breakup of ^{8}B.

The experimental data are displayed in Fig. 6. The three parts correspond to different bins of ^{7}Be-p relative energy after breakup: (a) $E = 0.5$–0.75 MeV, (b) $E = 1.25$–1.5 MeV, and (c) $E = 2.0$–2.25 MeV. Alongside the data are shown the results of our calculations. To allow a comparison with the data, they have been filtered by the experimental resolution provided by the authors of Ref. [7].

The full lines correspond to calculations performed with P-T interactions containing both Coulomb and nuclear potentials. The agreement with the data is fair, in particular at small scattering angle (i.e. $\theta < 6°$). Indeed both the magnitude and general feature of the data are well reproduced by our calculations. Note that no parameter adjustment has been done to fit the data. At larger angle, the theoretical calculation drops faster than the measurements. This could be due to an inappropriate choice of optical potentials to simulate the P-T nuclear interactions, which indeed are significant only at large scattering angle (see below). Another explanation of this discrepancy could be the filtering with the experimental resolution. Following Ogata *et al.* [20], it has been devised assuming the breakup of ^{8}B to occur only through an s continuum state. As shown by these authors this is not the case at large scattering angle [20]. Therefore the quantitative comparison between theory and experiment may not be significant for too large θ.

Note that our calculations are in perfect agreement with those of Ref. [20] (see Fig. 3 of that reference) although different reaction models and different ^{8}B descriptions are considered. This agreement validates both calculations. It also suggests that the details of the ^{8}B description have but little effect on these calculations. As for the parallel-momentum distributions (see Sec. IV A), a simple two-body model of ^{8}B seems sufficient to reproduce this breakup observable.

With the aim of analysing the influence of the nuclear P-T interactions, we also perform the dynamical calculation considering purely Coulomb P-T potentials. The corresponding angular distributions are displayed as dotted lines in Fig. 6. As observed for the parallel-momentum and energy distributions, the difference with the Coulomb plus nuclear calculation is negligible at forward angles (i.e. $\theta < 4$–$6°$). At larger angle on the contrary, the difference is more significant. The elastic breakup is strongly reduced in the Coulomb plus nuclear case, probably due to the absorption terms of the optical potentials. As mentioned earlier, this attenuation is not observed experimentally. It could be due to an inappropriate choice of the optical potentials, or to uncertainty in the filtering technique. The angle at which the difference appears between the purely Coulomb and Coulomb plus nuclear calculations decreases at larger relative energy E. This is in agreement with previous calculations, where it has been shown that nuclear potentials affect more significantly the breakup cross section at large relative energy [21, 40].

To complete this analysis of the influence of the nuclear interaction as well as to show the effect of the filtering on the distributions, we show in Fig. 7 the result of our calculations for the first relative-energy bin before filtering. The full line corresponds to the Coulomb plus nuclear P-T interactions. The dotted line is obtained with purely Coulomb interactions.

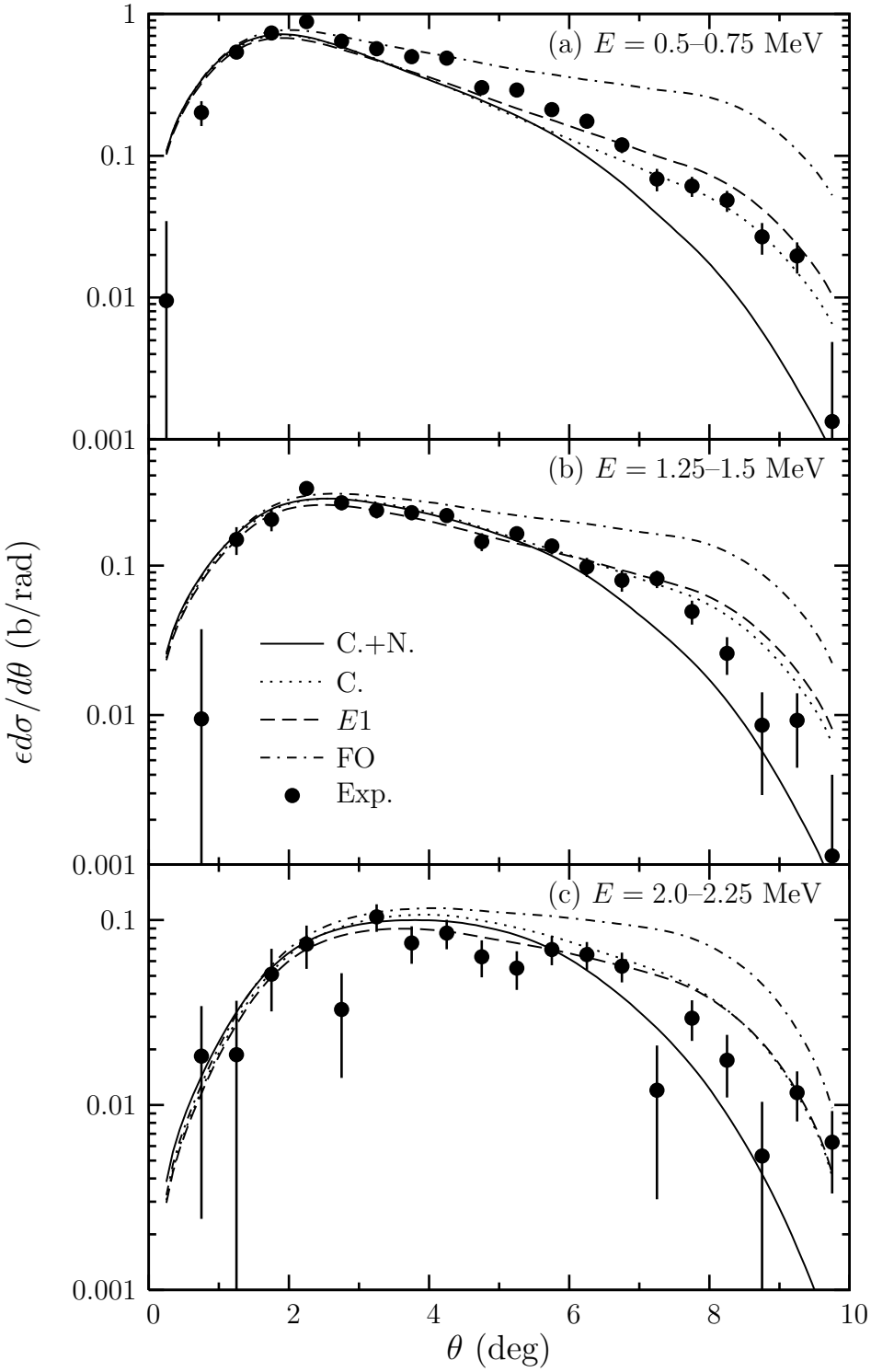

FIG. 6: Breakup of ^{8}B on Pb at 52 MeV/nucleon: angular distribution as a function of ^{8}B center-of-mass scattering angle θ. Three ranges for the ^{7}Be-p relative energy are considered: (a) $E = 0.5$–0.75 MeV, (b) $E = 1.25$–1.5 MeV, and (c) $E = 2.0$–2.25 MeV. DEA calculations are performed using Coulomb plus nuclear (full lines), purely Coulomb (dotted line), and $E1$ (dashed line) P-T interactions. First-order calculations performed with $E1 + E2$ strengths are shown as dash-dotted lines. Experimental data are from Ref. [7]. All distributions are convoluted with the experimental resolution.

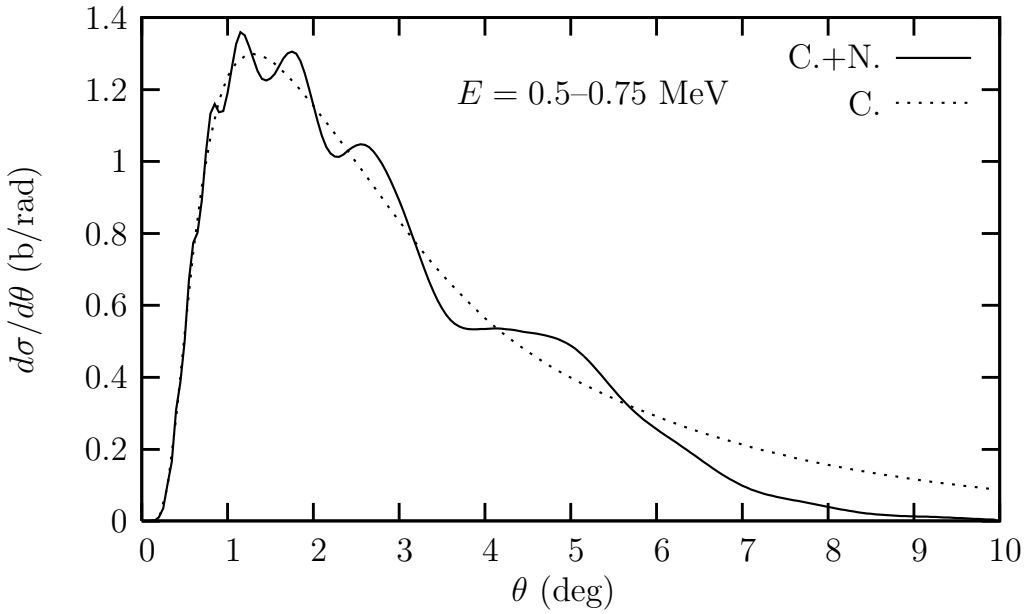

FIG. 7: Theoretical calculations of ^{8}B breakup on Pb at 52 MeV/nucleon. The angular distributions obtained for $E = 0.5$–0.75 MeV are not convoluted with the experimental resolution. dynamical calculations are performed using Coulomb plus nuclear (full lines) and purely Coulomb (dotted line) P-T interactions.

Both distributions exhibit the same magnitude for $\theta < 6°$. However, the former oscillates around the latter. This effect is a signature of the interferences between the solutions of Eq. (3) corresponding to neighboring impact parameters [26]. The absence of such oscillations in the purely Coulomb calculation shows that the presence of nuclear terms in the P-T potentials is responsible for this pattern, already observed by Ogata *et al.* (see Fig. 2 of Ref. [20]). The angular distribution is thus sensitive to nuclear interactions even at very forward angles. However the experimental angular resolution hides these interferences in the measurements. Once filtered, both theoretical distributions look very similar at forward angles (see Fig. 6). This result also explains that no effect of the nuclear interaction is observed in the parallel-momentum and energy distributions. In these cases, the integration over θ cancels out the oscillations. The angular distribution seems therefore a proper observable to bring out the influence of nuclear interactions. However this requires a very fine experimental resolution.

To evaluate the contribution of the quadrupole term of the Coulomb P-T interaction to the angular distribution, we also compute this observable using a purely $E1$ interaction. The corresponding calculations are displayed as dashed lines in Fig. 6. As observed for the energy distribution (see Fig. 4), these results are not significantly different from the purely Coulomb ones. The difference between both calculations indeed remains small in comparison with the size of the error bars and/or with the influence of the nuclear interaction. Moreover it varies with both the scattering angle and the relative energy. The $E1$ distribution can indeed be higher or lower than the total Coulomb one, confirming the energy dependence of the $E1$-$E2$ interferences mentioned earlier. Moreover, these results show the angular distribution to be an improper observable to analyse the influence of the $E2$ strength upon breakup, unlike the parallel momentum distribution.

We also compare the DEA with perturbation theory. The dash-dotted lines in Fig. 6 correspond to the first-order distribution obtained using the classical relation between the impact parameter b and the scattering angle θ. As for the energy distribution, the first-order approximation overestimates the dynamical calculation. This is particularly true at large scattering angle (i.e. small b in a semiclassical point of view), where perturbation theory is less valid. However even below 1°, the difference between the first-order and dynamical calculations remains of the order of 10%. This confirms the significant influence of higher-order effects in the dissociation process, and the difficulty of interpreting experimental data within the framework of first-order perturbation theory.

This analysis of the angular distributions indicates that like parallel-momentum distributions, this observable is relatively well described by our dynamical calculation using a rather simple description of the projectile. Angular distributions do not seem very sensitive to the projectile description. This result is confirmed by the similarity between our results and those of Ogata *et al.* , which are obtained with different models of ^{8}B [20]. Our analysis also shows that contrary to what was supposed by Kikuchi *et al*, this observable is not properly suited to extract the $E2$ contribution to the breakup. First there does not seem to be a range in angle where the breakup is $E2$ dominated. Second, as for the other observables, higher-oder effects play a significant role, which makes hypothetical the use of perturbation theory to analyse the data. On the contrary, it seems that angular distributions seem to be well suited to emphasize the effects of nuclear interaction in dissociation. An interference pattern indeed appears when optical potentials are included in the P-T interaction. Unfortunately, the detection of this pattern requires too fine a resolution to be observed experimentally in the available measurements.

D. On the extraction of the ^{7}Be$(p,\gamma)^8$B astrophysical S factor

All the aforementioned Coulomb breakup experiments have been performed with the final aim of determining the astrophysical S_{17} factor for the radiative capture ^{7}Be$(p,\gamma)^8$B at stellar energies. The analyses presented in the preceding sections show that the task is more complicated than initially suggested by Baur *et al.* [5]. The breakup process cannot be seen in these experiments as a mere one step $E1$ transition from the initial bound state to the continuum. If indeed the nuclear interaction between the projectile and the target can be suppressed by selecting data at forward angle, the presence of significant $E2$ strengths, and higher-order effects hinder the direct extraction of $B(E1)$ from the breakup data.

To circumvent these problems, one could think of using these measurements to constrain the ^{8}B description. However, our systematic analysis of various experiments shows that a crude description of ^{8}B is sufficient to explain most of the measurements. The mechanism of Coulomb breakup seems therefore well understood. However, this result also suggests that this reaction is not a very accurate probe of the structure of the projectile. A more realistic description of the projectile might not improve significantly the agreement with experiment, and therefore could hardly be constrained by such data.

As a first attempt to analyse the influence of the projectile description upon the breakup calculations, we have computed the energy distributions using three ^{7}Be-p potentials adjusted in the s wave to reproduce various scattering lengths $a_0 = 5.9$ fm, -2.8 fm, and -7 fm (see Sec. IV B). Unfortunately, none of the descriptions seems to better fit the data. We have observed a change only in the magnitude of the cross section (see Fig. 5). If information about the ^{8}B description were to be extracted from this analysis, a different

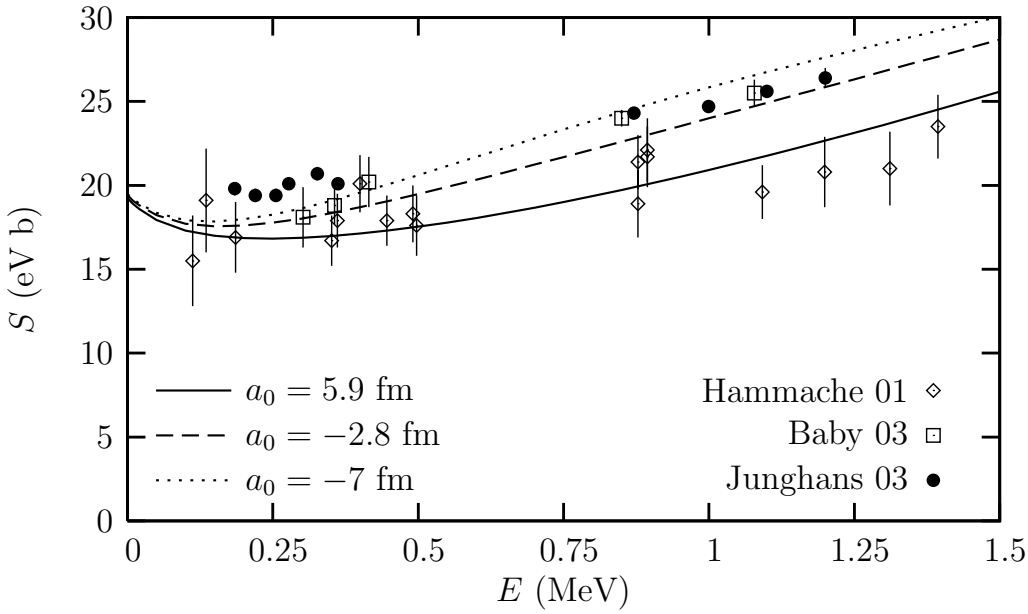

FIG. 8: Astrophysical S_{17} factor for the ^{7}Be$(p,\gamma)^8$B radiative capture. Calculations are performed with the three ^{8}B descriptions given in Sec. IV B, characterized by the scattering lengths $a_0 = 5.9$ fm (initial potential; full lines), $a_0 = -2.8$ fm (dashed lines), and $a_0 = -7$ fm (dotted lines). Experimental data are from Refs. [2, 3, 4].

normalisation factor would then be obtained for each potential.

To evaluate the influence of the ^{8}B model upon the radiative capture, we plot the S_{17} factor corresponding to each of the three potentials in Fig. 8 as a function of the ^{7}Be-p relative energy E. The results of three recent direct measurements are shown as well [2, 3, 4]. All three potentials lead to very similar S_{17} factors at zero energy: 19.2, 19.4, and 19.5 eV b, for $a_0 = 5.9$ fm (full line), -2.8 fm (dashed line), and -7 fm (dotted line) respectively. This is due to the tiny dependence of the astrophysical S_{17} factor on the scattering length at low energy [37]. The energy dependence of S_{17}, however, differs from one potential to the other. While it behaves rather smoothly with E in the $a_0 = 5.9$ fm case, it increases more rapidly when a_0 is negative. This smooth behavior is in agreement with the measurements of Hammache *et al.* [2], and Junghans *et al.* [4], although both sets of data differ in magnitude. The data of Baby *et al.* [3] seem better reproduced when S_{17} increases faster with the energy.

These results show that there remain significant uncertainties in the extraction of S_{17} at stellar energy from breakup data. In this indirect technique, the comparison between theory and experiment provides information at two levels. First it evaluates the ability of both the reaction and projectile-structure models to describe the breakup mechanism, i.e. to reproduce accurately the shape of the cross sections. Second, it gives a scaling factor from the adjustment of the magnitude of the theoretical cross section upon the experimental one. The S_{17} factor extracted from breakup would then be the theoretical S_{17} obtained from the ^{8}B model multiplied by this scaling factor. Our analysis shows that within the DEA, a crude two-body description of ^{8}B is able to reproduce fairly well the shape of most of the Coulomb breakup observables. However, as seen in Sec. IV B, different ^{8}B models, while leading to similar energy distributions, give different magnitudes of this cross section. Since these models lead to essentially the same theoretical S_{17} at zero energy (see Fig. 8), one

would extract, from that observable, a different S_{17} from each of these ^{7}Be-p potentials. We also see that even with one description of ^{8}B, different S_{17} could be extracted from Coulomb breakup data, depending on the observable considered. Indeed, the good agreement between theory and experiment for the parallel-momentum distribution at 44 MeV/nucleon (see Fig. 1) suggests a unit scaling factor. However, the DEA calculation performed with the same ^{8}B description overestimates the experimental parallel-momentum distribution at 81 MeV/nucleon by up to 10–25% (see Fig. 3), suggesting a scaling factor lower than one, and therefore a smaller S_{17} at zero energy.

The mechanism of the Coulomb breakup of ^{8}B seems now well understood. Most of the breakup observables are indeed well reproduced with the DEA considering a simple two-body model of the projectile. Nevertheless, efforts still need to be done to understand the discrepancies between theory and experiment in the magnitude of some cross sections. Since this magnitude is sensitive to the ^{7}Be-p scattering length, similar calculations involving a more realistic ^{8}B model (i.e. reproducing the measured scattering lengths, and therefore including the spin of the core) might solve this problem. The approximate treatment of special relativity used in the present breakup model (see Sec. II D) may also be an issue. To evaluate this effect, a comparison with a relativistic extension of the DEA is needed. Such an extension is planned in the near future. However, the recent results obtained by Bertulani with a relativistic extension of the CDCC technique do not suggest this effect to be significant at intermediate energies [42]. Until then the extraction of the astrophysical S_{17} factor from breakup data will be subjected to uncertainty no smaller than that obtained from direct measurements.

V. CONCLUSION

The cross section of the radiative capture reaction $^7\mathrm{Be}(p,\gamma)^8\mathrm{B}$ is one of the key inputs to calculate accurately the flux of high-energy neutrinos produced in the sun. The difficulty of its direct measurement has raised interests in indirect techniques. It has been proposed to infer the astrophysical S_{17} factor at stellar energies from cross sections of the Coulomb breakup of ^{8}B [5]. Several experiments have been performed with this aim [6, 7, 8, 9, 10, 11].

Unfortunately, the extraction of S_{17} from the breakup of ^{8}B is not straightforward. While radiative capture is purely $E1$ dominated, breakup includes a non-negligible $E2$ strength [8, 12]. Moreover higher-order effects in the Coulomb breakup process may hinder this extraction [12]. Finally, the projectile-target nuclear interaction, albeit small, might spoil the dissociation data.

In this paper, we analyse various ^{8}B Coulomb breakup sets of data [7, 8, 10] within a single reaction model (the dynamical eikonal approximation [25, 26]) considering a single description of ^{8}B. This description is based on a simple ^{7}Be-p potential model, in which the spin of the core is neglected. Although very crude, this description seems sufficient to reproduce most of the breakup observables, computed within the DEA. We indeed obtain a good agreement with experiment for angular and longitudinal momentum distributions in both shape and magnitude. Albeit fair, the agreement is less good for the energy distribution, possibly because of an insufficiently realistic ^{8}B description.

To analyse the breakup mechanism and its sensitivity to projectile-target interactions, we systematically perform all calculations with various projectile-target potentials.

First the calculations are done with optical potentials that simulate both Coulomb and nuclear interactions. To analyse the influence of the nuclear interaction on the data, they

are compared to calculations performed with purely Coulomb potentials. In most of the cases the difference is found negligible if distributions are limited to very forward angles. The influence of nuclear interactions can thus be avoided in Coulomb breakup.

Second, we compare the breakup observables obtained with either the full Coulomb interaction or only its dipole term. For all cross sections, we observe differences, but only for the parallel-momentum distribution are they significant. In that distribution, the $E1$ calculation exhibits a reverse asymmetry compared to the full Coulomb one, confirming the sensitivity of that observable to the $E2$ strength revealed in previous works [8, 12, 19, 31].

Finally, with the aim of analysing the significance of higher-order effects, we compare our dynamical calculation with first-order perturbation theory [35]. In agreement with previous analyses [17, 24], we observe significant couplings inside the continuum leading to interferences between $E1$ and $E2$ first-order transitions. These interferences lead to a reduction of the asymmetry of the parallel-momentum distributions, as observed in Refs. [8, 12, 15, 19, 31].

It seems therefore difficult to infer the accuracy of the astrophysical S_{17} factor extracted from breakup measurements as suggested in Ref. [5]. If indeed the projectile-target nuclear interaction can be neglected by selecting forward scattering angles, the non-negligible $E2$ contribution, and the presence of significant higher-order effects limit the reliability of this extraction. An unresolved issue is the influence of the ^{8}B description upon breakup calculations. The currently available data do not seem to suggest such a significant effect. But, perhaps the limited experimental acceptance hides some interesting effects. Therefore, future works are planned to evaluate the interplay between the structure of ^{8}B and its dissociation. This requires an improvement of the projectile description within the DEA. If breakup turned out to be a useful probe of the structure of ^{8}B, it could serve to constrain a more precise ^{8}B model. Subsequently, this model could provide a reliable extrapolation of S_{17} down to low energies.

Acknowledgments

This text presents research results of the Belgian program P6/23 on interuniversity attraction poles initiated by the Belgian-state Federal Services for Scientific, Technical and Cultural Affairs (FSTC). G. G. acknowledges the support of the FRIA, Belgium. P. C. acknowledges the support of the Fund for Scientific Research (F. R. S.-FNRS), Belgium.

APPENDIX A: FIRST-ORDER PERTURBATION THEORY

By using the first-order perturbation theory to solve the time-dependent Schrödinger equation the breakup amplitudes used in Eq. (8) are given by [35]

$$\begin{aligned} S_{kljm}^{(m_0)E\lambda}(b) \;=\; & \frac{1}{i\hbar} Z_T Z_{\text{eff}}^{(\lambda)} \frac{e^2}{4\pi\epsilon_0} e^{i(\sigma_l+\delta_{lj}-l\pi/2)} (-1)^{I-m_0} \sqrt{\frac{4\pi}{2\lambda+1}} I_{\lambda\ m_0-m} \\ & \times \sqrt{(2l_0+1)(2j_0+1)(2l+1)(2j+1)} \begin{pmatrix} l & \lambda & l_0 \\ 0 & 0 & 0 \end{pmatrix} \begin{Bmatrix} j & l & I \\ l_0 & j_0 & \lambda \end{Bmatrix} \\ & \times \begin{pmatrix} j_0 & \lambda & j \\ m_0 & m-m_0 & -m \end{pmatrix} \int_0^\infty u_{klj}(r) r^\lambda u_{n_0 l_0 j_0}(r) dr, \end{aligned} \tag{A1}$$

where $\omega = (E - E_0)/\hbar$, and the effective charge $Z_{\rm eff}^{(\lambda)}$ is defined by

$$Z_{\rm eff}^{(\lambda)} = \left(-\frac{m_c}{m_P}\right)^{\lambda} Z_f + \left(\frac{m_f}{m_P}\right)^{\lambda} Z_c. \tag{A2}$$

For straight line trajectories, the time integral $I_{\lambda\mu}$ {see e.g. Eq. (13) of Ref. [24]} in Eq. (A1) can be evaluated analytically [41]

$$I_{\lambda\mu} \;=\; \sqrt{\frac{2\lambda+1}{4\pi}}\frac{2}{v}\frac{i^{\lambda+\mu}}{\sqrt{(\lambda+\mu)!(\lambda-\mu)!}}\left(\frac{\omega}{v}\right)^{\lambda} K_{|\mu|}\left(\frac{\omega b}{v}\right), \tag{A3}$$

where K_n is a modified Bessel function [27].

APPENDIX B: FRAME TRANSFORMATION

The core and fragment momentum in the laboratory frame are defined in spherical coordinates by $\boldsymbol{p_c} = (p_c, \theta_c, \varphi_c)$ and $\boldsymbol{p_f} = (p_f, \theta_f, \varphi_f)$ while the total momentum $\boldsymbol{p}_{tot}$ is assumed to be in the Z-direction. The energy and momentum conservation laws lead to the following relation

$$\begin{aligned} & p_f^2\left(\frac{1}{2m_f}+\frac{1}{2m_T}\right) - \frac{p_f}{m_T}\left(P_{tot}\cos\theta_f - p_c\sin\theta_f\sin\theta_c\cos\Delta\varphi - p_c\cos\theta_f\cos\theta_c\right) \\ & + \left[\frac{p_c^2}{2m_c} - E_{tot} + \frac{1}{2m_T}(p_{tot}^2 + p_c^2 - 2p_{tot}p_c\cos\theta_c)\right] = 0, \end{aligned} \tag{B1}$$

where E_{tot} is the total energy in the laboratory frame. The fragment momentum p_f can thus be deduced from p_c, θ_c, θ_f and $\Delta\varphi = \varphi_c - \varphi_f$. ¿From Eqs. (12) and (13), one obtains in the center of mass frame, the relative momentum between the fragment and the core

$$\hbar^2 k^2 = \left(\frac{m_c}{m_P}\right)^2 p_f^2 + \left(\frac{m_f}{m_P}\right)^2 p_c^2 - 2\frac{m_f m_c}{m_P^2} p_f p_c \left(\sin\theta_f\sin\theta_c\cos\Delta\varphi + \cos\theta_f\cos\theta_c\right), \tag{B2}$$

the corresponding colatitude

$$\cos\theta_k = \frac{m_c p_f\cos\theta_f - m_f p_c\cos\theta_c}{m_P\hbar k}, \tag{B3}$$

the relative momentum between the projectile and the target

$$\begin{aligned} \hbar^2 K'^2 \;=\; & p_c^2 + p_f^2 + 2p_c p_f\sin\theta_c\sin\theta_f\cos\Delta\varphi + 2p_c p_f\cos\theta_c\cos\theta_f \\ & + \left(\frac{m_P}{m_T+m_P}\right)^2 p_{tot}^2 - 2\frac{m_P}{m_T+m_P} p_{tot}(p_c\cos\theta_c + p_f\cos\theta_f), \end{aligned} \tag{B4}$$

the corresponding colatitude

$$\cos\theta = \frac{p_c\cos\theta_c + p_f\cos\theta_f - \frac{m_P}{m_T+m_P}p_{tot}}{\hbar K'}, \tag{B5}$$

and the difference between the two azimuthal angles

$$\tan(\varphi - \varphi_k) = \frac{\sin\Delta\varphi}{\frac{m_c}{m_P}\frac{p_f \sin\theta_f}{p_c \sin\theta_c} - \frac{m_f}{m_P}\frac{p_c \sin\theta_c}{p_f \sin\theta_f} + \frac{m_c - m_f}{m_P}\cos\Delta\varphi}. \tag{B6}$$

The three-body phase space factor is given by [29]

$$\rho(E_c, \Omega_c, \Omega_f) = \frac{m_c m_f m_T p_c p_f}{(2\pi\hbar)^6}\Big[m_T + m_f + \frac{m_f}{p_f}(p_c \sin\theta_f \sin\theta_c \cos\Delta\varphi + p_c \cos\theta_f \cos\theta_c - p_{tot}\cos\theta_f)\Big]^{-1}. \tag{B7}$$

---

[1] J. N. Bahcall, *Neutrino Astrophysics* (Cambridge University Press, Cambridge, 1989).

[2] F. Hammache, G. Bogaert, P. Aguer, C. Angulo, S. Barhoumi, L. Brillard, J. F. Chemin, G. Claverie, A. Coc, M. Hussonnois, M. Jacotin, J. Kiener, A. Lefebvre, C. L. Naour, S. Ouichaoui, J. N. Scheurer, V. Tatischeff, J. P. Thibaud, and E. Virassamynaiken, Phys. Rev. Lett. **86**, 3985 (2001).

[3] L. T. Baby, C. Bordeanu, G. Goldring, M. Hass, L. Weissman, V. N. Fedoseyev, U. Koster, Y. Nir-El, G. Haquin, H. W. Gaggeler, R. Weinreich, and the ISOLDE Collaboration, Phys. Rev. Lett. **90**, 022501 (2003).

[4] A. Junghans, E. Mohrmann, K. Snover, T. Steiger, E. Adelberger, J. Casandjian, H. Swanson, L. Buchmann, S. Park, A. Zyuzin, and A. Laird, Phys. Rev. C **68**, 065803 (2003).

[5] G. Baur, C. A. Bertulani, and H. Rebel, Nucl. Phys. **A458**, 188 (1986).

[6] T. Motobayashi, N. Iwasa, Y. Ando, M. Kurokawa, H. Murakami, J. Ruan, S. Shimoura, S. Shirato, N. Inabe, M. Ishihara, T. Kubo, Y. Watanabe, M. Gai, R. H. France, K. I. Hahn, Z. Zhao, T. Nakamura, T. Teranishi, Y. Futami, K. Furutaka, and T. Delbar, Phys. Rev. Lett. **73**, 2680 (1994).

[7] T. Kikuchi, T. Motobayashi, N. Iwasa, Y. Ando, M. Kurokawa, S. Moriya, H. Murakami, T. Nishio, J. Ruan (Gen), S. Shirato, S. Shimoura, T. Uchibori, Y. Yanagisawa, T. Kubo, H. Sakurai, T. Teranishi, Y. Watanabe, M. Ishihara, M. Hirai, T. Nakamura, S. Kubono, M. Gai, R. France III, K. Hahn, T. Delbar, P. Lipnik, and C. Michotte, Phys. Lett. B **391**, 261 (1997).

[8] B. Davids, D. W. Anthony, S. M. Austin, D. Bazin, B. Blank, J. Caggiano, M. Chartier, H. Esbensen, P. Hui, C. Powell, H. Scheit, B. Sherrill, M. Steiner, P. Thirolf, J. Yurkon, and A. Zeller, Phys. Rev. Lett. **81**, 2209 (1998).

[9] V. Guimarães, J. J. Kolata, D. Peterson, P. Santi, R. H. White-Stevens, S. M. Vincent, F. D. Becchetti, M. Y. Lee, T. W. O'Donnell, D. A. Roberts, and J. A. Zimmerman, Phys. Rev. Lett. **84**, 1862 (2000).

[10] B. Davids, D. W. Anthony, T. Aumann, S. M. Austin, T. Baumann, D. Bazin, R. R. C. Clement, N. C. Davids, H. Esbensen, P. A. Lofty, T. Nakamura, B. M. Sherrill, and J. Yurkon, Phys. Rev. Lett. **86**, 2750 (2001).

[11] F. Schümann, S. Typel, F. Hammache, K. Sümmerer, F. Uhlig, I. Böttcher, D. Cortina, A. Förster, M. Gai, H. Geissel, U. Greife, E. Grosse, N. Iwasa, P. Koczo, B. Kohlmeyer, R. Kulessa, H. Kumagai, N. Kurz, M. Menzel, T. Motobayashi, H. Oeschler, A. Ozawa, M. Posko, W. Prokopowicz, E. Schwab, P. Senger, F. Strieder, C. Sturm, Z.-Y. Sun, G. Surówka, A. Wagner, and W. Waluś, Phys. Rev. C **73**, 015806 (2006).

[12] H. Esbensen and G. F. Bertsch, Nucl. Phys. **A600**, 37 (1996).
[13] S. Typel and G. Baur, Phys. Rev. C **50**, 2104 (1994).
[14] R. Shyam and I. J. Thompson, Phys. Rev. C **59**, 2645 (1999).
[15] B. Davids and S. Typel, Phys. Rev. C **68**, 045802 (2003).
[16] S. Typel, H. H. Wolter, and G. Baur, Nucl. Phys. **A613**, 147 (1997).
[17] H. Esbensen, G. F. Bertsch, and K. A. Snover, Phys. Rev. Lett. **94**, 042502 (2005).
[18] J. A. Tostevin, F. M. Nunes, and I. J. Thompson, Phys. Rev. C **63**, 024617 (2001).
[19] J. Mortimer, I. J. Thompson, and J. A. Tostevin, Phys. Rev. C **65**, 064619 (2002).
[20] K. Ogata, S. Hashimoto, Y. Iseri, M. Kamimura, and M. Yahiro, Phys. Rev. C **73**, 024605 (2006).
[21] P. Capel, D. Baye, and V. S. Melezhik, Phys. Rev. C **68**, 014612 (2003).
[22] V. S. Melezhik and D. Baye, Phys. Rev. C **59**, 3232 (1999).
[23] V. S. Melezhik and D. Baye, Phys. Rev. C **64**, 054612 (2001).
[24] P. Capel and D. Baye, Phys. Rev. C **71**, 044609 (2005).
[25] D. Baye, P. Capel, and G. Goldstein, Phys. Rev. Lett. **95**, 082502 (2005).
[26] G. Goldstein, D. Baye, and P. Capel, Phys. Rev. C **73**, 024602 (2006).
[27] M. Abramowitz and I. Stegun, *Handbook of Mathematical Functions* (Dover, New-York, 1970).
[28] Note the typo in Eq. (45) of Ref. [26], where the factor $i^{|m-m_0|}$ is wrongly placed at the numerator. The correct expression of the breakup transition matrix element is given by Eq. (8).
[29] H. Fuchs, Nucl. Instrum. Methods Phys. Res. **200**, 361 (1982).
[30] D. Baye, P. Descouvemont, and N. Timofeyuk, Nucl. Phys. **A577**, 624 (1994).
[31] B. Davids, S. M. Austin, D. Bazin, H. Esbensen, B. M. Sherrill, I. J. Thompson, and J. A. Tostevin, Phys. Rev. C **63**, 065806 (2001).
[32] C. Angulo, M. Azzouz, P. Descouvemont, G. Tabacaru, D. Baye, M. Cogneau, M. Couder, T. Davinson, A. D. Pietro, P. Figuera, M. Gaelens, P. Leleux, M. Loiselet, A. Ninane, de F. Oliveira Santos, P. G. Pizzone, R. Ryckewaert, de N. Sereville, and F. Vanderbist, Nucl. Phys. **A716**, 211 (2003).
[33] J. Cook, Nucl. Phys. **A388**, 153 (1982).
[34] F. D. Becchetti and Jr. G. W. Greenlees, Phys. Rev. **182**, 1190 (1969).
[35] K. Alder and A. Winther, *Electromagnetic Excitation* (North-Holland, Amsterdam, 1975).
[36] B. Davids, (private communication), (2007).
[37] D. Baye, Phys. Rev. C **62**, 065803 (2000).
[38] S. Typel and G. Baur, Nucl. Phys. **A759**, 247 (2005).
[39] P. Capel and F. M. Nunes, Phys. Rev. C **73**, 014615 (2006).
[40] S. Typel and R. Shyam, Phys. Rev. C **64**, 024605 (2001).
[41] H. Esbensen and C. A. Bertulani, Phys. Rev. C **65**, 024605 (2002).
[42] C. A. Bertulani, Phys. Rev. Lett. **94**, 072701 (2005).